

Bond order densities in real space

José Luis Casals-Sainz, A. Fernández-Alarcón, Evelio Francisco, Aurora Costales,
and Ángel Martín Pendás*

Departamento de Química Física y Analítica. Universidad de Oviedo. 33006 Oviedo. Spain.

E-mail: ampendas@uniovi.es

Abstract

In this contribution we introduce the concept of bond order density (BOD) based on previous work on natural adaptive orbitals. We show that BODs may be used to visualize both the global spatial distribution of the covalent bond order as well as its eigen-components, which we call bond(ing) channels. BODs can be equally computed at correlated and non-correlated levels of theory, and in ground or excited states, thus offering an appealing description of bond-forming, bond-breaking, and bond-evolution processes. We show the power of the approach by examining a number of homo- and hetero-diatomics, including the controversial existence of a fourth bonding component in dicarbon, by analyzing a few interesting bonding situations in polyatomics and chemical transformations, and by exemplifying exotic bonding behaviors in simple excited electronic states.

Introduction

The theory of chemical bonding in real space,¹ a framework that provides an orbital invariant alternative to the dominant orbital dependent paradigm,² is being progressively enriched with a battery of tools that provide a map between the concepts of the two approaches. Both the electron counting and the energetic faces of chemical bonding are covered. Within the first category one can now obtain reliable covalent³ and ionic⁴ bond orders at any level of theory, free from the inherent arbitrariness of *manually* selecting which (natural) orbitals are to be considered bonding or antibonding.⁵ These bond orders can be spectrally analyzed^{6,7} – a process that uncovers their elementary constituents (i.e. individual bonds) – in two- as well as in multicenter bonding scenarios. A natural bond orbital (NBO)-like decomposition from quantum atoms has also been proposed,^{8,9} and through the use of electron distribution functions¹⁰ resonance structures can be invariantly recovered. As energetics is regarded, orbital-free energy decompositions that lead to chemically intuitive atomic deformation energies and to pairwise additive covalent and ionic interactions are being used more and more.^{11,12}

Amongst the interesting connections that these techniques have uncovered, the literal equiva-

lence between covalency as a classical sharing of electrons, and delocalization viewed as a mutual fluctuation (covariance) of atomic electron populations, stands out. When electrons delocalize between two centers the populations of the latter become statistically dependent, and a covalent contribution to the interaction energy sets in. The covalent bond order is just a measure of the number of electrons (or electron pairs) that delocalize, as quantified by their covariance.¹³

An intriguing aspect of the real space view of covalency that has not been fully addressed yet is its spatial distribution, i.e. which spatial regions contribute more intensely in building up a given bond order or covalent strength. We show herein how a bond order density (BOD) can be defined and partitioned into bonding channels. Examining the total bond order density as well as its eigen-contributions in representative systems offers interesting clues about bonding mechanisms. In many cases, the real space picture is in good agreement with traditional orbital images. Sometimes it may either support or refute recent controversial claims. Finally, in the case of excited states or of heavily correlated systems, it provides truly new insights.

As we will see, the BOD here defined has formally the same expression at the Hartree-Fock (HF) and correlated (i.e. multideterminantal) levels when it is expressed in terms of the natural adaptive orbitals (NAdOs).^{6,14} This fact makes it possible to compare on an equal basis mean field and correlated results. Moreover, although in this work we will only show BODs for two-fragment partitions of molecular systems, the formalism is general and can be applied to other bonding patterns, e.g. to multicenter two-electron bonds (nc,2e).

We have divided the article as follows. We firstly show, using the H₂ molecule as an example, that a direct analysis of the spatial distribution of the bond order leads to interesting but difficult to generalize results. Then, the concept of bond order density (BOD), much more suitable for this purpose, is introduced based of the previous definition of natural adaptive orbitals (NAdOs),^{6,14} and some computational details about its implementation given. After this, the BOD results for a set of main group homodiatomics and heterodiatomics are presented and discussed, the evolution of BOD in a couple of chemical processes analyzed and the BOD results on several polyatomic molecules discussed. Finally, we show that the usefulness of the BOD concept is not restricted

to the ground state, but it can also be applied to excited electronic states. The article ends with a summary and the main conclusions of our work.

On the spatial extension of electron delocalization

In real space approaches to chemical bonding, 3D regions are associated to chemical objects like atoms, cores, lone pairs, functional groups, etc. Although this can be done in several ways,¹² we choose here the atomic partition provided by the quantum theory of atoms in molecules (QTAIM),¹⁵ which enjoys a solid theoretical foundation. It is well established that the covalent energy associated to the interaction between two quantum atoms A and B is¹⁶

$$E_{cov}^{AB} = - \int_A d\mathbf{r}_1 \int_B d\mathbf{r}_2 \frac{\rho_c^2(\mathbf{r}_1, \mathbf{r}_2)}{r_{12}}, \quad (1)$$

where each electron coordinate is integrated over one of the spatial atomic domains of the two atoms and ρ_c^2 is the second-order cumulant (or exchange-correlation) density (2CD), $\rho_c^2(\mathbf{r}_1, \mathbf{r}_2) = \rho(\mathbf{r}_1)\rho(\mathbf{r}_2) - \rho_2(\mathbf{r}_1, \mathbf{r}_2)$, with ρ and ρ_2 being the one- and two-particle densities, respectively. The 2CD integrates to N , the total number of electrons, and

$$\text{DI}(A, B) = \delta^{AB} = 2 \int_A d\mathbf{r}_1 \int_B d\mathbf{r}_2 \rho_c^2(\mathbf{r}_1, \mathbf{r}_2), \quad (2)$$

called the delocalization index or covalent bond order, measures how many electrons are shared between both domains.¹⁷ It can be shown that $\delta^{AB} = -2\text{cov}(n_A, n_B)$, the covariance of the joint distribution that describes the probability of finding a given number of electrons in each atom.¹⁸

How is, for instance, δ^{AB} distributed in space? A first glimpse can be obtained by examining the H_2 molecule at the single-determinant, i.e. HF level, that provides $\delta = 1$. In this case it can easily be verified that $\rho_c^2 = \rho(\mathbf{r}_1)\rho(\mathbf{r}_2)/2$, and this shows that the integrand in Eq. 2 peaks when each electron lies on top of each of the nuclei. This behavior, that is easily rationalized if we take into account that the probability of finding an electron is maximum at the nuclei, clashes

with the classical picture where it is the build-up of electron density between the two nuclei the driving force behind chemical binding. Although it is obviously true that bonding leads to such a density build-up, and that the internuclear density accumulation plays an important role in the overall energy balance, it is clear from the previous argument that the electrons that are shared in a simple covalent interaction tend to be close to the atomic nuclei, and that a properly defined bond order density must reflect this.

This said, it can also be readily shown that the delocalization leading to the unit bond order in H_2 extends through all the space. Taking into account that the two atoms are separated by the plane that bisects the internuclear axis at its middle point, further insight can be obtained by introducing two extra ancillary planes, parallel to the interatomic surface, that pass through each of the two nuclei (see Fig. 1). The integral in Eq. 2 has then four components ($A_1B_1, A_1B_2, A_2B_1, A_2B_2$). Ignoring the abovementioned density accumulation, each of the four regions contributes approximately the same amount to δ , so that the internuclear region is only responsible for about a fourth of the total bond order.

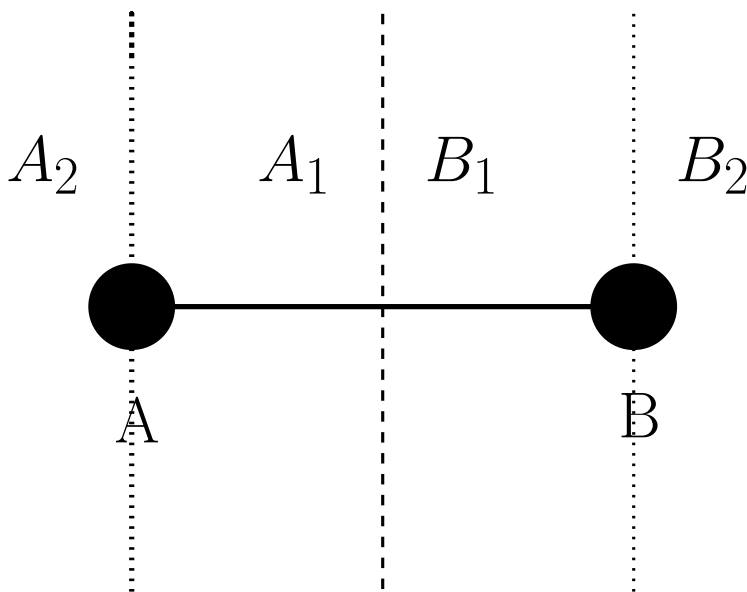


Figure 1: Projection of the interatomic surface (dashed) and ancillary planes (dotted) for the H_2 molecule on a plane passing through the nuclei.

This situation is in a sense extreme since in polyatomic polyelectron molecules the bonding

electrons are usually more localized due to Pauli exclusion with other electrons. The previous argument nevertheless shows that the spatial distribution of the delocalization may not fulfil our expectations.

Interesting as these arguments are, Eq. 2 is not useful from the practical point of view, since it involves a two-particle integrand difficult to visualize. It would be rather more convenient to transform its integrand into a standard one-particle density. This has already been done, and we succinctly revisit in the following section the theoretical arguments leading to such a one-particle BOD or bonding density.

Natural adaptive domain orbitals, bond order densities and bond order channels

We have shown in the past how a hierarchical set of general bonding indices can be derived^{6,14} through the joint use of further order reduced density matrices (RDMs) and real space partitions. Key in this methodology are the n -th order cumulant densities (nCDs), which carry information about true n -body correlations. nCDs enjoy several important properties, among which we notice their size extensivity and their recursivity. They are simply that part of the n -th order reduced densities (nRDs) which cannot be written in terms of lower order RDs. They integrate to the total number of electrons N , and if condensed over the coordinates of one electron they recover the $(n-1)$ CD,

$$\begin{aligned} \rho_c^{n-1}(\mathbf{r}_1, \dots, \mathbf{r}_{n-1}) &= \int d\mathbf{r}_n \rho_c^n(\mathbf{r}_1, \dots, \mathbf{r}_n) \\ \int d\mathbf{r}_1 \dots d\mathbf{r}_n \rho_c^n(\mathbf{r}_1, \dots, \mathbf{r}_n) &= N. \end{aligned} \quad (3)$$

Similar expressions can be written for the non-diagonal cumulant density matrices.

Since it has been shown^{13,19,20} that n -center bonding emerges from n -center fluctuations of atomic populations, the condensation of a nCD over n different atomic domains provides the num-

ber of electrons (out of the grand total N) engaged in n -center bonding, so that the n -center populations

$$N_{ab\dots n} = \int_{\Omega_a} d\mathbf{r}_1 \int_{\Omega_b} d\mathbf{r}_2 \cdots \int_{\Omega_n} d\mathbf{r}_n \rho_c^n(\mathbf{r}_1, \dots, \mathbf{r}_n) \quad (4)$$

are simple invariant measures of n -center delocalization. These quantities, properly normalized, are called n -center delocalization indices. For instance, twice the two-center one is the standard DI defined above.

The use of the 3CD or the 3CDM allows to define a one-particle density that integrates to $N_{ab} = \delta^{AB}/2$,

$$\rho_{ab}(\mathbf{r}_1) = \int_{\Omega_a} d\mathbf{r}_2 \int_{\Omega_b} d\mathbf{r}_3 \rho_c^3(\mathbf{r}_1, \mathbf{r}_2, \mathbf{r}_3). \quad (5)$$

Notice that $\sum_{a,b} \rho_{ab}(\mathbf{r}) = \rho(\mathbf{r})$, so that the electron density has been decomposed into localized and delocalized contributions. Moreover, the equivalently defined density matrix $\rho_{ab}(\mathbf{r}'_1, \mathbf{r}_1)$ can be diagonalized and written as a sum of one particle contributions, $\rho_{ab}(\mathbf{r}'_1, \mathbf{r}_1) = \sum_i n_{ab}^i \phi_i^*(\mathbf{r}'_1) \phi(\mathbf{r}_1)$. We have called these ϕ functions Natural Adaptive Orbitals (NAdOs).⁶ They have been shown to faithfully recover standard orbital knowledge in single determinant descriptions and to offer valuable information in correlated cases.²¹

The quantity that we will use in the following, $2\rho_{ab}(\mathbf{r})$, is a bond order density that has not been appropriately explored so far, and that can be further decomposed into a set of independent bonding channels (the $2n_{ab}^i |\phi_i(\mathbf{r})|^2$ contributions). In the mean-field approximation $\rho_{ab}(\mathbf{r})$ can be written as¹⁴

$$\rho_{ab}(\mathbf{r}) = \sum_{i,j} \varphi_i^*(\mathbf{r}) D^{ab} \varphi_j(\mathbf{r}), \quad (6)$$

where $D^{ab} = S^a S^b + S^b S^a$, φ_i are the canonical orbitals, and S^a and S^b are the atomic overlap matrices (AOM) in A and B , respectively, defined by $S_{ij}^a = \langle \varphi_i | \varphi_j \rangle_A$ and $S_{ij}^b = \langle \varphi_i | \varphi_j \rangle_B$. If real space is divided into only two domains A and B (so that $A \cup B = \mathcal{R}^3$), D^{ab} becomes equal to $2S^a(I - S^a)$, with its eigenvalues given by $2n_{ab}^i = 2s_i^a(1 - s_i^a)$, where the s_i^a 's are the eigenvalues of S^a . Since the latter is positive definite, all s_i^a 's and (consequently) n_{ab}^i 's are positive. Hence, in the mean field approximation, $\rho_{ab}(\mathbf{r})$ is positive everywhere. Same-spin (Fermi) correlation, taken into

account in the mean-field approximation, always gives rise to positive BODs. This is no longer true if (Coulomb) electron correlation is included. In this case $D^{ab} \neq S^a S^b + S^b S^a$ and ρ_{ab} may be negative and display negative channels; i.e. some of the eigenvalues of D^{ab} are negative and dominate over the positive ones in some parts of the 3D space, resulting in a negative value of $\rho_{ab}(\mathbf{r})$. These negative regions will indicate a predominance of Coulomb over Fermi correlation. Although they are small and the overall DI is positive, negative bond orders have indeed been found in excited states.²² These are truly new situations where traditional bonding analyses may fail.

Implementation and computational Details

Bond order densities and channels have been obtained through our in-house code DENMAT,²³ which is a general purpose program to build and analyze nCDs from externally computed wavefunctions. Its basic input is a standardized description of the wavefunction together with the AOMs between all occupied and virtual orbitals, obtained through our also in-house PROMOLDEN program.²⁴ Only results from multiconfigurational calculations will be analyzed, although some comparisons with HF calculations will be offered. We have chosen a representative subset of homo- and heterodiatomics, a few polyatomics and some relevant excited states to show the power of the approach.

Since our prescription looks to uncover bonding patterns more than to quantitatively describe systems, we have resorted to a complete active space (CASSCF) level of theory. Fine details that depend on dynamical correlation, like accurate dissociation energies or relative stabilities, are not appropriately modeled at this level, but the most important bonding factors are well described. Active spaces were selected using a modified Atomic Valence Active Space (AVAS)³⁰ procedure, where core orbitals are excluded from the projecting step and a splitting of the threshold used for the occupied and virtual sets is taken into account. Geometries were not optimized in general but taken from the literature instead. More details can be found in Tables 1, 2 and 3. The BN

Table 1: Atomic valence active space (AVAS) and details for homodiatomic molecules studied in this work. A threshold of 0.1 e was used for orbital occupations in the occupied space and of $10^{-5} e$ for the virtual space. The geometry of C_2^{2-} and B_2^{2-} was optimized as described in the text.

Molecule	Distance (Å)	State	Impurities	Active Space
H ₂	0.7414 ²⁵	$1\Sigma_g^+$	1s	2e,3o
Li ₂	2.6730 ²⁵	$1\Sigma_g^+$	2s,2p	2e,9o
Be ₂	2.4600 ²⁵	$1\Sigma_g^+$	2s,2p	4e,10o
B ₂	1.5900 ²⁵	$3\Sigma_g^-$	2s,2p	6e,12o
C ₂	1.2425 ²⁵	$1\Sigma_g^+$	2s,2p	8e,12o
N ₂	1.0976 ²⁵	$1\Sigma_g^+$	2s,2p	10e,13o
O ₂	1.2075 ²⁵	$3\Sigma_g^-$	2s,2p	12e,15o
F ₂	1.4119 ²⁵	$1\Sigma_g^+$	2s,2p	14e,15o
Na ₂	3.0789 ²⁵	$1\Sigma_g^+$	3s,3p	2e,9o
Mg ₂	3.8905 ²⁵	$1\Sigma_g^+$	3s,3p	4e,10o
Si ₂	2.2460 ⁵	$1\Sigma_g^+$	3s,3p,4s,4p	8e,20o
P ₂	1.8934 ²⁵	$1\Sigma_g^+$	3s,3p	10e,13o
S ₂	1.8890 ⁵	$3\Sigma_g^-$	3s,3p	12e,15o
Cl ₂	1.9879 ²⁵	$1\Sigma_g^+$	3s,3p	14e,15o
K ₂	3.9051 ²⁵	$1\Sigma_g^+$	4s,4p	2e,9o
Ca ₂	4.2773 ²⁵	$1\Sigma_g^+$	4s,4p	4e,10o
Ge ₂	2.3680 ⁵	$1\Sigma_g^+$	4s,4p,5s,5p	8e,20o
As ₂	2.1030 ⁵	$1\Sigma_g^+$	4s,4p	10e,13o
Se ₂	2.1660 ⁵	$3\Sigma_g^-$	4s,4p	12e,15o
Br ₂	2.2810 ²⁵	$1\Sigma_g^+$	4s,4p	14e,15o
C_2^{2-}	1.2907	$1\Sigma_g^+$	2s,2p	10e,13o
B_2^{2-}	1.7048	$1\Sigma_g^+$	2s,2p	8e,12o

singlet was chosen at the same geometry of the triplet. In all the cases the Sapporo-QZP-2012 basis sets³¹ augmented with diffuse basis functions were used. Most of the electronic structure calculations were performed using the PySCF suite.³² In the case of the HCN path the active space was found at the transition state and then propagated to reactants and products to ensure a consistent description along the complete IRC.

In the case of C_2^{2-} and B_2^{2-} the geometry was optimized at the CASSCF level using the first twelve orbitals in each case and using only the valence electrons with an aug-cc-pVTZ basis set³³. At this level of theory the equilibrium distances of C_2 and B_2 match well the experimental values, so that we deem our geometries accurate enough. The same procedure was applied for the optimization of BC^- , with the first twelve orbitals and valence electrons. The geometries of the

Table 2: AVAS active space and details for heterodiatomic molecules studied in this work. A threshold of 0.1 was used for the occupied space and 10^{-5} for the virtual space. The geometry of BC^- was optimized as described in the text.

Molecule	Distance (Å)	State	Impurities	Active Space
BeO	1.3309 ²⁵	$^1\Sigma^+$	Be 2s,2p;O 2s,2p	8e,12o
BeS	1.7415 ²⁵	$^1\Sigma^+$	Be 2s,2p;S 3s,3p	8e,12o
MgO	1.7490 ²⁵	$^1\Sigma^+$	Mg 3s,3p;O 2s,2p	8e,12o
MgS	2.1425 ²⁵	$^1\Sigma^+$	Mg 3s,3p;S 3s,3p	8e,12o
CaO	1.8211 ²⁵	$^1\Sigma^+$	Ca 4s,4p;O 2s,2p	8e,12o
CaS	2.3177 ²⁵	$^1\Sigma^+$	Ca 4s,4p;S 3s,3p	8e,12o
CO	1.1282 ²⁵	$^1\Sigma^+$	C 2s,2p;O 2s,2p	10e,13o
CO ⁺	1.1152 ²⁵	$^2\Pi$	C 2s,2p;O 2s,2p	9e,13o
SiO	1.5097 ²⁵	$^1\Sigma^+$	Si 3s,3p;O 2s,2p	10e,13o
GeO	1.6242 ²⁵	$^1\Sigma^+$	Ge 4s,4p;O 2s,2p	10e,13o
CS	1.5349 ²⁵	$^1\Sigma^+$	C 2s,2p;S 3s,3p	10e,13o
CSe	1.6762 ²⁵	$^1\Sigma^+$	C 2s,2p;Se 4s,4p	10e,13o
SiS	1.9293 ²⁵	$^1\Sigma^+$	Si 3s,3p;S 3s,3p	10e,13o
BF	1.2669 ²⁶	$^1\Sigma^+$	B 2s,2p;F 2s,2p	10e,13o
BCl	1.7159 ²⁵	$^1\Sigma^+$	B 2s,2p;Cl 3s,3p	10e,13o
BO ⁺	1.2040 ²⁷	$^1\Sigma^+$	B 2s,2p;O 2s,2p	8e,12o
BO	1.2045 ²⁷	$^2\Sigma^+$	B 2s,2p;O 2s,2p	9e,13o
BO ⁻	1.2360 ²⁷	$^1\Sigma^+$	B 2s,2p;O 2s,2p	10e,13o
BS	1.6092 ²⁵	$^2\Sigma^+$	B 2s,2p;S 3s,3p	9e,13o
NO ⁺	1.0657 ²⁸	$^1\Sigma^+$	N 2s,2p;O 2s,2p	10e,13o
NO ⁻	1.2580 ²⁸	$^3\Sigma^-$	N 2s,2p;O 2s,2p	12e,15o
AlO	1.6179 ²⁵	$^2\Sigma^+$	Al 3s,3p;O 2s,2p	9e,13o
AlS	2.0290 ²⁵	$^2\Sigma^+$	Al 3s,3p;S 3s,3p	9e,13o
BeF	1.3610 ²⁹	$^2\Sigma^+$	Be 2s,2p;F 2s,2p	9e,13o
BeCl	1.7971 ²⁵	$^2\Sigma^+$	Be 2s,2p;Cl 3s,3p	9e,13o
SO	1.4811 ²⁵	$^3\Sigma^-$	S 3s,3p;O 2s,2p	12e,15o
SeO	1.6395 ²⁵	$^3\Sigma^-$	Se 4s,4p;O 3s,3p	12e,15o
SeS	2.0467 ²⁵	$^3\Sigma^-$	Se 4s,4p;S 3s,3p	12e,15o
GaO	1.7430 ²⁵	$^1\Sigma^+$	Ga 4s,4p;O 2s,2p	9e,13o
GeSe	2.1350 ²⁵	$^1\Sigma^+$	Ge 4s,4p;Se 4s,4p	10e,13o
AsN	1.6184 ²⁵	$^1\Sigma^+$	As 4s,4p;N 2s,2p	10e,13o
PN	1.4909 ²⁵	$^1\Sigma^+$	P 3s,3p;N 2s,2p	10e,13o
BC	1.4912 ²⁵	$^4\Sigma^-$	B 2s,2p,3s,3p;C 2s,2p,3s,3p	7e,21o
BC ⁻	1.3865	$^1\Sigma^+$	B 2s,2p,3s,3p;C 2s,2p,3s,3p	8e,20o
BN	1.3250	$^1\Sigma^+$	B 2s,2p,3s,3p;N 2s,2p,3s,3p	8e,20o
CN ⁺	1.1590 ²⁵	$^1\Sigma^+$	C 2s,2p,3s,3p;N 2s,2p,3s,3p	8e,20o
CN	1.1718 ²⁵	$^2\Sigma^+$	C 2s,2p,3s,3p;N 2s,2p,3s,3p	9e,21o
CN ⁻	1.1770 ²⁵	$^1\Sigma^+$	C 2s,2p,3s,3p;N 2s,2p,3s,3p	10e,21o

Table 3: AVAS active space and details for other molecules studied in this work. A threshold of 0.1 e was used for the occupied space and $10^{-5}i$ e for the virtual space. The distance refers to C–C, Si–Si, and N→B, respectively, in the first three molecules, and to C–N in CH₂N₂ and HCN.

Molecule	Distance (Å)	State	Impurities	Active Space
C ₂ H ₂	1.2026 ²⁵	¹ Σ _g ⁺	C 2s,2p	12e,20o
Si ₂ H ₂	2.2449	¹ A _g	Si 3s,3p	10e,13o
NH ₃ →BH ₃	1.6453 ²⁵	¹ A ₁	B 2s,2p;N 2s,2p	14e,15o
CH ₂ N ₂	1.2875	¹ A ₁	C 2s,2p;N 2s,2p	16e,17o
HCN	1.1714	¹ A _v	C 2s,2p;N 2s,2p	10e,13o

Si₂H₂ and CH₂N₂ molecules were optimized at the HF level with the aug-cc-pVTZ³³ basis set, and the intrinsic reaction coordinate (IRC) for the HCN \longleftrightarrow CNH interconversion was found at the HF level using the GAMESS³⁴ code and the aug-cc-pvdz basis set.³³ The transition state structure and the optimized geometries are included in the electronic supplementary information (ESI) as xyz files. The optimized structures were subsequently used to perform a CASSCF analysis at each point. In the case of CO and CS dissociation paths, the active space was determined at the equilibrium geometry of each molecule and then used for all geometries throughout the path.

The wavefunctions of the electronic excited states of H₂ were obtained with the Molpro³⁵ code. We have selected the B¹Σ_u⁺ (S1) and the double minimum E,F¹Σ_g⁺ (S2) states at the MRCI-SD level of theory, with a two-orbital 10-electron reference obtained from a state averaged wavefunction (SA-CASSCF) with the d-aug-cc-pVDZ³³ basis set. As a second example, we have taken the D_{4h} H₄ molecule in the ¹A_{1g} excited state at the FCI level using the aug-cc-pvdz basis set. The PySCF suite³² was used in this case with a distance between closest H atoms equal to 1.2 Å.

As commented, PROMOLDEN²⁴ was used to obtain the AOMs and several interacting quantum atoms (IQA) quantities. Numerical integrations were performed using β -spheres with radii between 0.1 and 0.3 bohr. Restricted angular Lebedev quadratures with 3074 points and 451 points Gauss-Chebyshev mapped radial grids were used inside the β -spheres, with l expansions cut at $l = 8$. Outside the β -spheres, extended 5810-point Lebedev, 551 mapped radial point Gauss-Legendre quadratures, and l expansions up to $l = 10$ were selected. Where necessary, electron distribution functions were obtained with EDF.³⁶

Bonding densities in main group homodiatomics

We have examined the first to fourth row main group homodiatomics in their experimental ground states, with geometries taken mostly from the NIST²⁵ database. Full details about interatomic distances, electronic states and active spaces can be found in the ESI. Noble gas diatomics have been excluded since their DIs are very small and higher levels of theory together with extremely fine numerical integrations would be needed to obtain reliable results. Table 4 shows the total DI, the covalent and classical AB interaction energies, and the number of main contributions to δ for the studied homodiatomeric molecules. In Table 5 we gather the occupation numbers (i.e. the contributions to the total DI) of the dominant bonding channels. In all cases, each NAdO can be mapped to a natural orbital (NO) of the full system. By doing so, the pair formed by the contribution of the NAdO to the DI and the occupation of its twin NO provides an enhanced information about this bonding channel. In order to build an easy to follow narrative, only dominant channels (here defined as those with a NO occupation number greater than $0.1 e$) will be discussed. In H_2 , as already noticed,⁶ there is an overwhelmingly dominant σ contribution which accounts for 99% the total DI. The bond order density (BOD) view is compatible with that offered in our first direct dihydrogen example: each of the four regions A_1, A_2, B_1 , and B_2 display a grossly equal contribution to the four $(A_1B_1, A_1B_2, A_2B_1, A_2B_2)$ pairs, so all of them contribute a similar value to the DI. This is also what happens if we integrate the σ_g NAdO in those spatial domains.

Second row homodiatomics

The second row diatomics show an interesting evolution of the total DI as well as of the number and type of dominant channels. The DI in Li_2 (the zero-flux surface has been forced to be a plane at the internuclear midpoint) is very similar to that in H_2 , although its leading term is significantly smaller, and a number of minor correlating NAdOs appear (the occupation of the twin NO to the leading NAdO is only $1.81 e$). A color map showing the evolution of the BOD for H_2, Li_2 , and the remaining homodiatomics of this series is plotted in Fig. 2. Notice that, due to the long R_e value in

Li₂, the BOD is very delocalized and small in the internuclear region. Passing to Be₂ the low $2s$ - $2p$ gap induces a considerable multiconfigurational character. Although the $2\sigma_g$ and $2\sigma_u$ orbitals interfere destructively (as in traditional accounts), they do not at all cancel out. A relatively strong 0.37σ channel survives, and a pair of correlated NAdOs⁶ appear. The correlating partner has a non-negligible negative n_{ab} value that gives rise to negative BOD regions in the overall map. This is an exo-bond, in line with findings from the natural bond order formalism,³⁷⁻⁴⁰ or from valence bond (VB) theory.⁴¹ Notice how an energetically very weak link, like that in Be₂, may involve a non-negligible multiple bond character. Several very weak, but distinct channels can be present.

The exo-bond persists as a dominant channel in B₂ and C₂. In these systems the 2π orbital block becomes populated. The contribution of π channels to the DI, as expected, tends to be smaller than that of the leading σ channel when correlation is included. This asymmetry decreases at small R_e 's. The leading σ channel strengthens on increasing Z , while the exo-bond loses intensity due to a larger correlating partner (with negative eigenvalue). Be that as it may, both in B₂ and C₂ there are four distinct bonding channels, in agreement with both NBO and recent non-orthogonal VB results.⁴¹ We stress that the four components are already present at the HF level (we have also included the HF results for C₂ in Table 5) and that electron correlation affects the HF exo-bond (the $2\sigma_u$ canonical orbital) considerably, decreasing its n_{ab} value. Regardless its energetic track, a formalism independent from VB, like the one presented here, finds four clear bonding components in dicarbon. Just as a short digression, an equivalent calculation in acetylene finds no hint of the exo-bond. This is compatible with a model in which two unpaired electrons in the C₂ fragment are either used to form the two C–H links in acetylene, leading to no exo-bond, or forced to couple as a singlet in dicarbon. This extra coupling in the same spatial region reduces the strength of the first σ component, since the correlating partner of the exo-bond is negative in the internuclear region. In fact, the n_{ab} value of the σ channel in C₂H₂ is significantly larger than in C₂. These conclusions are reinforced by calculations in the B₂²⁻ and C₂²⁻ systems, which are isoelectronic to C₂ and N₂, respectively. Transforming dicarbon into a dinitrogen isoelectronic analogue makes the exo-bond disappear and increases the σ n^{ab} . The contrary is true in diboron.

In N_2 two extra electrons are added onto the σ symmetry sector, and the 2σ channels get blocked. Only one σ component survives (the canonical $3\sigma_g$ orbital), leading to the purest case of triple bond available in the series. Even in this case, electron correlation has a big impact on the effective bond order, with $2n_{ab}$ values considerably smaller than one. The introduction of two extra electrons in dioxygen partially blocks the 2π sector (we are presenting a spinless picture). Finally, in difluorine the π electrons are almost blocked and only a σ component remains. The decrease in the σn_{ab} value along the dinitrogen to difluorine sequence is related to the increase in R_e and to Sanderson’s lone pair bond weakening effect (LPBWE).⁴² In this case, there are small, but non-negligible contributions from the π electrons (lone pairs).

Table 4: Values of the total delocalization index δ^{AB} , covalent (E_{Cov}) and classical (E_{Cl}) interaction energy components, and number of bonding channels (NBC) or main contributions to δ^{AB} for the homodiatomic molecules.

Molecule	δ^{AB}	E_{Cov}	E_{Cl}	NBC
H_2	0.8351	-0.2294	0.0420	1
Li_2	0.8344	-0.1003	0.0019	1
Be_2	0.5867	-0.0930	0.0050	2
B_2	1.3835	-0.3243	0.0467	4
C_2	1.8419	-0.5523	0.1413	4
N_2	2.0299	-0.7159	0.2271	3
O_2	1.5870	-0.5058	0.1464	3
F_2	0.9207	-0.2572	0.0515	1
Na_2	0.7655	-0.0801	0.0003	1
Mg_2	0.2336	-0.0262	0.0004	2
Si_2	1.3833	-0.2714	0.0273	2
P_2	1.8877	-0.4424	0.0577	3
S_2	1.5855	-0.3929	0.0594	3
Cl_2	1.1197	-0.2783	0.0428	1
K_2	0.7778	-0.0688	0.0007	1
Ca_2	0.4401	-0.0455	0.0007	2
Ge_2	1.3333	-0.2471	0.0131	2
As_2	1.7847	-0.3783	0.0417	3
Se_2	1.4909	-0.3262	0.0372	3
Br_2	1.0787	-0.2388	0.0290	1
C_2^{2-}	2.2278	-0.5543	0.2188	3
B_2^{2-}	2.0045	-0.3196	0.1435	4

A look to the BOD maps is instructive and visually appealing. H_2 shows a relatively compact density with a prolate shape. The midpoint of the internuclear axis (MP) is a minimum of the BOD,

Table 5: Dominant bonding channels of main group homodiatomics. A channel is considered dominant if its associated natural orbital has an occupation greater than 0.1 e . Occupation numbers of the twin natural orbital (in parenthesis) are shown. Whenever a correlated companion with a non-negligible negative occupation is found, it is also shown in a second row. In acetylene, the C–C link has been analyzed.

	σ	exo – σ	$\pi_x = \pi_y$
H ₂	0.8226(1.97)	-	-
Li ₂	0.7550(1.81)	-	-
Be ₂	0.3721(1.86)	0.2024(1.71)	-
	-	-0.0394(0.17)	-
B ₂	0.6160(1.95)	0.1954(1.66)	0.3322(0.97)
	-	-0.0896(0.31)	-
C ₂	0.6772(1.97)	0.1815(1.62)	0.5608(1.88)
	-	-0.0882(0.38)	-
C ₂ (HF)	0.3000(2.00)	0.3000(2.00)	1.0000(2.00)
N ₂	0.7898(1.99)	-	0.6201(1.94)
O ₂	0.7362(1.99)	-	0.3878(1.95)
F ₂	0.6476(1.90)	-	-
Na ₂	0.6977(1.82)	-	-
Mg ₂	0.1253(1.87)	0.1122(1.84)	-
	-	-0.0113(0.06)	-
Si ₂	0.6205(1.29)	-	0.3463(1.24)
P ₂	0.7595(1.98)	-	0.5680(1.90)
S ₂	0.7146(1.93)	-	0.3963(1.95)
Cl ₂	0.7274(1.93)	-	-
K ₂	0.6922(1.78)	-	-
Ca ₂	0.2522(1.84)	0.1768(1.78)	-
	-	-0.0261(0.10)	-
Ge ₂	0.6220(1.40)	-	0.3227(1.18)
As ₂	0.7378(1.94)	-	0.5312(1.89)
Se ₂	0.6897(1.93)	-	0.3687(1.94)
Br ₂	0.7159(1.92)	-	-
C ₂ ²⁻	0.7933(1.97)	-	0.6608(1.91)
B ₂ ²⁻	0.5565(1.92)	0.2229(1.72)	0.6604(1.83)
	-	-0.0920(0.24)	-
C ₂ H ₂	0.7450(1.98)	-	0.5845(1.93)

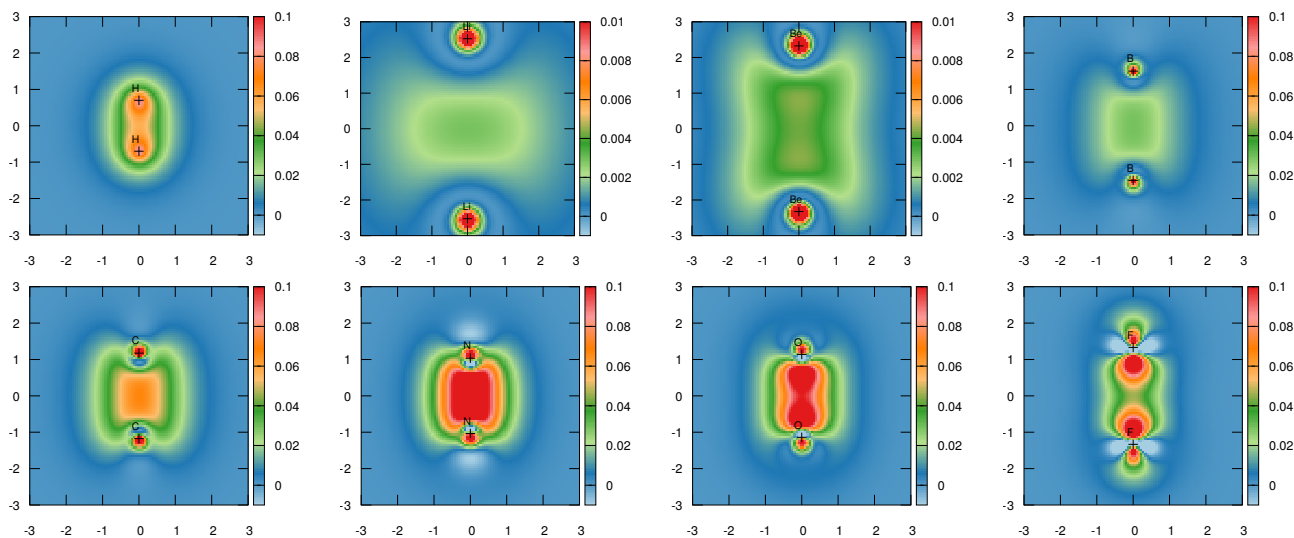


Figure 2: Bond order density maps for the $Z = 1, 3 - 5$ (top) and $Z = 6 - 9$ (bottom) diatomics. The color scale has been chosen so that both positive and negative regions are clearly highlighted. Nuclear positions are marked with crosses, and distances and isodensity values are shown in au.

with a value of 0.057 au. On the contrary, the distribution in Li_2 is much more disperse and oblate, and it needs a zoomed scale to be properly seen. The link with the existence of a non-nuclear attractor in this case should be further studied. The MP is now a maximum with $\text{BOD} = 0.003$ au. In Be_2 this maximum splits into two, and the MP is a $(3, -1)$ critical point with $\text{BOD} = 0.004$ au. In B_2 the presence of π contributions is clear, and again a maximum of the $\text{BOD} = 0.029$ au at the MP appears that persists in C_2 ($\text{BOD} = 0.067$ au), where a clear region with negative densities starts to be observed. From N_2 to F_2 the MP is again a $(3, -1)$ point, with $\text{BOD} = 0.144, 0.100, 0.046$ au, respectively. Notice that this sequence resembles the structure of the laplacian of the electron density.¹⁵ The change in topology on going from B_2 to F_2 coincides with the traditional inversion in the filling order of the canonical molecular orbitals occurring at dinitrogen and with the change from mainly s -like to p_z -like of the character of the σ channel. This coincides with a transition from a convex to a concave disposition of the BOD in the internuclear region. Moreover, going from dinitrogen to difluorine evinces a tendency to re-localization, so that F_2 displays obvious features of a proto-bond, as it has been already proposed.⁴³ Truly novel insights come from examining the negative regions in the maps, that correspond to failures of the one-particle picture. As seen, they exist in all the B_2 to F_2 molecules, changing from σ -like to π -like symmetry on dioxygen. A visual

identification of the regions that oppose to bonding due to correlation effects is thus possible. The weakening role of the fluorine lone pairs is in this way pictorially available.

In addition to the full BOD maps, it is also possible to visualize specific bonding channels whose analysis can also provide valuable information about the pattern of bonds in the molecule. For instance, the maps associated to the $\text{exo-}\sigma$ channel with positive occupation of Be_2 , B_2 , and C_2 molecules, plotted in Fig. 3 and included also in the ESI, show that their positive regions are mainly concentrated at the rear part of the atomic nuclei. The bonding $\text{exo-}\sigma$ channels in our BOD approach are formed when there exists the possibility of exciting electrons from the 2s to the 2p orbital. In these three molecules they have a diradical character, with one electron in the back part of each the nuclei of the molecule. Although, for brevity, we will not discuss the exo-bond in as much detail as in the present case for heterodiatomics, it is worth commenting that its diradical character may be different from that found here, as both electrons are concentrated in some cases on the back part of the same nucleus.

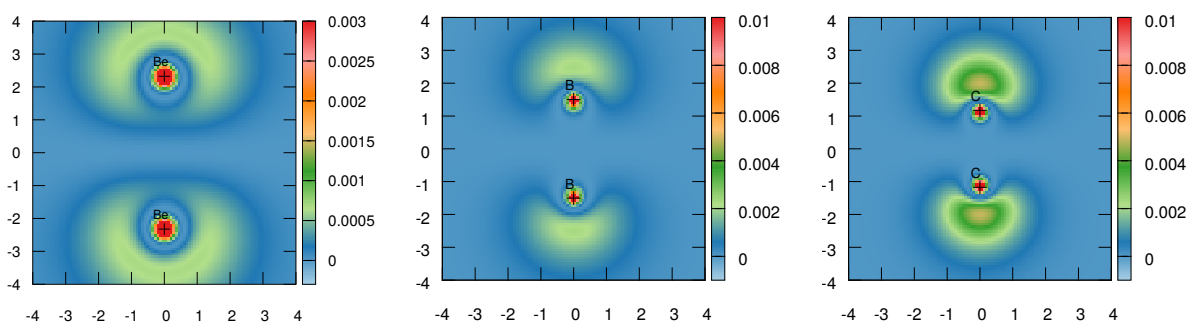


Figure 3: $\text{Exo-}\sigma$ bonding channel with a positive occupation of Be_2 (left), B_2 (center), and C_2 (right) molecules. Notice that the scale used in Be_2 is different from that in B_2 and C_2 .

Third and fourth row homodiatomics

If we move to the third and fourth rows, we need first to take into account that although the symmetry of the states in Si_2 and Ge_2 coincides with that in C_2 their orbital structure is different. Actually, the $3\sigma_g$ (Si_2) and $4\sigma_g$ (Ge_2) canonical orbitals lie below the valence π block, so they are open shell singlets. Their orbital filling is thus similar to that of dinitrogen. The presence of the

third p_z -like valence σ contribution blocks almost completely the valence ns channels.

The use of more diffuse electron shells for bonding purposes decreases the effective overlap. Moreover, the multiconfigurational character of the states decreases slightly on going from the second to the third row, to increase a bit again in the fourth row. We can see this head of the group effect by examining NO occupations in Table 5.

Exo-bonds persist in the Mg_2 and Ca_2 molecules, although their negative correlating contributions are smaller than those found for the second row homodiatomics. Contrarily to C_2 , the exo-bond disappears for Si_2 and Ge_2 .

As a general rule, the intensity of both the σ and π channels decrease down a group, and π terms become more and more disfavoured with respect to σ ones. Nonetheless, there are notable exceptions to this rule that deserve further comment. For instance, the three group 2 homodiatomics (Be_2 , Mg_2 , Ca_2) display a σ and an exo- σ contribution, but their occupations show a minimum in Mg_2 which needs further analyses.

In the rest of the anomalies it is a channel of the head of the group which displays a too low contribution to the DI. For instance, in the tetrel group, as already commented, the σ contribution is too low in dicarbon due to the interference with the large exo-bond, as a comparison with acetylene, which lacks the exo contribution, shows. Similarly, in the chalcogen group the π channel in dioxygen is too small as is the σ one in the halogen group. The last two cases point toward the LPBWE.

The BOD maps for the third row are found in Fig. 4, and those of the fourth row diatomics in the ESI. In most cases, the features found in the second period are reproduced here, although the density values are smaller. The character of the MP critical point does not change on changing period, e.g. all alkaline and alkaline-earth display $(3, -3)$ and $(3, -1)$ points at the MP. Only in the N group P_2 and As_2 now show a $(3, -3)$ point. This shows that the tendency toward proto-bonding decreases as we run through a group, as expected. We have not included Al_2 and Ga_2 due to problems in the convergence of the CAS calculation to the desired electronic state.

Heterodiatomic molecules

Many of the concepts explored in homodiatomics are kept intact in heterodiatomics. We have examined, among others, second to fourth row chalcogenides and halides. The results are summarized in Tables 6 and 7, and relevant BODs shown in Fig. 5. In most cases, the full valence set of orbitals are engaged in bonding in a non-trivial way. Beryllium compounds exemplify our main points. The σ channel decreases its intensity as polarity is enhanced. This is the expected behavior, compatible with Pauling's insights and with the modern view provided by EDFs,⁴ which shows that, on a single channel, covalency and ionicity oppose each other. The exo-bond is present in all cases, although with a very low negative correlating partner. Its contribution to the DI is greatest in the second row, just as in the homodiatomic case. It is particularly interesting that each π contribution is almost as strong as the σ one in BeO, and that the joint contribution of both π channels in BeO and BeS outweighs the σ one.

The evolution of the bonding pattern on traversing a group is now exemplified by the CO, SiO, and GeO series. The exo-bond loses strength as we go from C to Ge, but it is considerably more important than in the homologous tetrel diatomics. On the contrary, the σ and π contributions are weaker in SiO than in CO and GeO.

A direct comparison between homo- and cross-diatomics is also instructive. We can do this with the trios (C_2, CO, O_2) and (Si_2, SiS, S_2). The behavior of the σ component is clearly Pauling-like, controlled by the difference in electronegativity. The evolution of the π terms is very sensitive to the compactness of the overall electron distribution, which is σ -dominated. In this way, the total π contribution of CO or SiS is in between those of the corresponding homodiatomics. Nevertheless, care needs to be taken, since the number of classical π links in O_2 or S_2 is one. With this in mind, the π skeleton is also subjected to polarity induced weakening.

Some features on the BOD maps are revealing. To consider just a few oxides, neat polarization differences are evidenced in Fig. 5. In homodiatomics, each nuclear region hosts areas of large positive and negative densities. However, in heterodiatomics the behavior of the nuclear areas discriminates the most electronegative partner, which is embedded in a negative region, from the

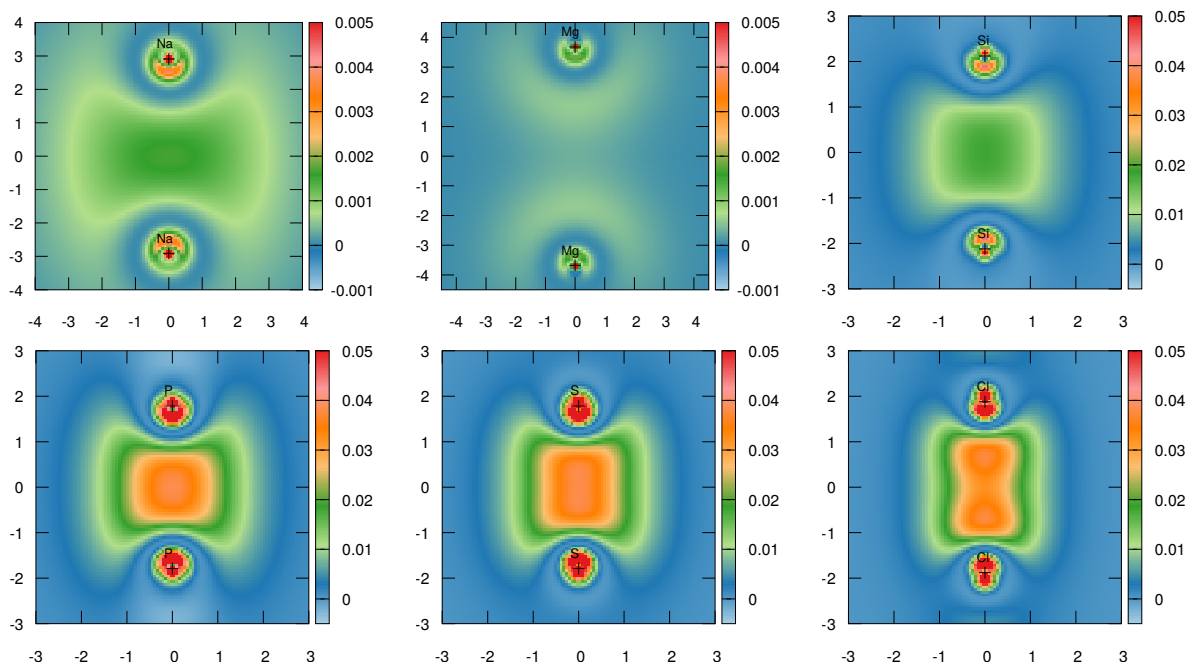


Figure 4: Bond density maps (left to right, top to bottom) for the third row diatomics excluding dioneon. The color scale has been chosen so that both positive and negative regions are clearly highlighted. Nuclear positions are marked with crosses, and distances and isodensity values are shown in au.

less electronegative element, where the contrary becomes true. The σ -like negative regions around oxygens are very clear, and the overall change in polarity on going from CO to CS appealing. We will examine this case in more detail below.

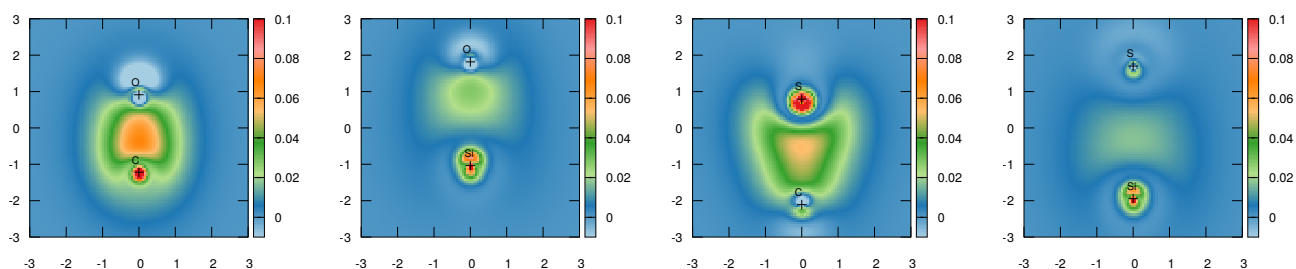


Figure 5: Bond density maps (left to right, top to bottom) for the CO, SiO, CS and SiS molecules. The color scale has been chosen so that both positive and negative regions are clearly highlighted. Nuclear positions are marked with crosses, and distances and isodensity values are shown in au.

Table 6: Values of the total delocalization index δ^{AB} , covalent (E_{Cov}) and classical (E_{Cl}) interaction energy components, net atomic charges (Q_a, Q_b), and number of bonding channels (NBC) or main contributions to δ^{AB} for the heterodiatomic molecules.

Molecule	δ^{AB}	E_{Cov}	E_{Cl}	Q_a	Q_b	NBC
CO	1.4384	-0.4362	-1.3700	1.2315	-1.2322	4
CO ⁺	1.4935	-0.4750	-1.2979	1.8594	-0.8587	3
SiO	1.0985	-0.2485	-1.2295	1.5076	-1.5076	4
GeO	1.3264	-0.3015	-0.5917	1.1286	-1.1284	3
CS	1.8586	-0.5022	-0.6111	-0.8517	0.8518	3
SiS	1.3085	-0.2658	-0.8295	1.2311	-1.2318	4
CSe	1.7706	-0.4460	-0.0686	-0.4421	0.4416	4
BeO	0.7156	-0.1602	-1.0750	1.6108	-1.6110	3
BeS	0.8846	-0.1709	-0.8246	1.4583	-1.4583	3
MgO	0.6821	-0.1138	-0.4039	1.0796	-1.0796	3
MgS	0.9283	-0.1407	-0.4010	1.1858	-1.1860	3
CaO	1.0688	-0.2063	-0.5729	1.3992	-1.3997	3
CaS	1.0093	-0.1585	-0.4700	1.4045	-1.4048	3
BF	0.7390	-0.1826	-0.7183	0.9147	-0.9148	4
BCl	0.8425	-0.1899	-0.5381	0.7883	-0.7885	4
BO ⁺	1.2553	-0.3292	-1.2973	2.0688	-1.0688	4
BO	1.0867	-0.2840	-1.3905	1.4974	-1.4977	4
BO ⁻	1.1769	-0.2734	-1.1211	0.7064	-1.7051	4
BS	1.3000	-0.3122	-0.7814	1.1251	-1.1247	3
NO ⁺	1.7542	-0.6384	-0.3777	1.2798	-0.2798	3
NO ⁻	1.6289	-0.4692	0.0505	-0.2796	-0.7204	3
AlO	0.9897	-0.1933	-0.9124	1.4653	-1.4657	3
AlS	1.1081	-0.2004	-0.6864	1.3197	-1.3205	3
BeF	0.4493	-0.0986	-0.5069	0.9408	-0.9417	2
BeCl	0.4917	-0.0938	-0.4328	0.9063	-0.9069	2
SO	1.4540	-0.3866	-1.0467	1.1485	-1.1481	3
SeO	1.4361	-0.3533	-0.4659	0.8924	-0.8922	3
SeS	1.5503	-0.3481	0.0023	0.2539	-0.2542	3
GeSe	1.5370	-0.3075	-0.1692	0.6743	-0.6744	3
GaO	1.2268	-0.2459	-0.3737	1.0009	-1.0010	4
CN ⁺	1.5630	-0.4979	-0.6671	1.4776	-0.4776	4
CN	1.7206	-0.5295	-0.8222	1.0478	-1.0466	4
CN ⁻	1.7413	-0.5131	-1.0173	0.6069	-1.6082	4
BN	1.3322	-0.3325	-0.8470	1.1828	-1.1827	4
BC	1.1247	-0.2702	-0.6229	0.9248	-0.9247	4
BC ⁻	1.5651	-0.3596	-0.6228	0.5402	-1.5400	4
PN	1.6612	-0.4051	-1.3597	1.4524	-1.4528	3
AsN	1.7327	-0.4107	-0.4617	0.9484	-0.9485	3

Table 7: Dominant bonding channels of heterodiatomic molecules. A channel is considered dominant if its associated natural orbital has an occupation greater than 0.1 e . Occupation numbers of the twin natural orbital (in parenthesis) are shown.

Molecule	σ	exo- σ	$\pi_x = \pi_y$
CO	0.4095(1.98)	0.2090(1.97)	0.4691(1.95)
CO ⁺	0.4879(1.94)	-	0.5261(1.93)
SiO	0.3212(1.97)	0.1601(1.91)	0.3469(1.95)
GeO	0.4843(1.96)	-	0.4177(1.93)
CS	0.6809(1.98)	-	0.5865(1.92)
SiS	0.4220(1.96)	0.1583(1.94)	0.4270(1.93)
CSe	0.7297(1.99)	0.1005(1.93)	0.5270(1.92)
GeSe	0.6244(1.98)	-	0.4719(1.93)
BeO	0.2865(1.98)	-	0.2356(1.95)
BeS	0.4366(1.93)	-	0.2625(1.94)
MgO	0.4218(1.66)	-	0.1107(1.96)
MgS	0.6179(1.86)	-	0.1743(1.95)
CaO	0.5236(1.94)	-	0.2666(1.96)
CaS	0.5666(1.93)	-	0.2226(1.96)
BO ⁺	0.5171(1.93)	0.1015(1.98)	0.4234(1.94)
BO	0.3299(1.97)	0.1335(1.00)	0.3502(1.95)
BO ⁻	0.2811(1.97)	0.3427(1.96)	0.3089(1.95)
BS	0.4973(1.94)	-	0.4165(1.93)
AlO	0.4698(1.95)	-	0.2495(1.95)
AlS	0.5220(1.94)	-	0.2932(1.94)
GaO	0.5552(1.94)	0.1095(1.00)	0.3104(1.95)
NO ⁺	0.6303(1.99)	-	0.5765(1.93)
NO ⁻	0.7301(1.98)	-	0.3813(1.96)
CN ⁺	0.5025(1.97)	0.1522(1.61)	0.5255(1.88)
CN	0.5722(1.97)	0.1285(1.02)	0.5565(1.91)
CN ⁻	0.5225(1.97)	0.1601(1.94)	0.5779(1.93)
BN	0.4454(1.70)	0.1373(1.97)	0.4522(1.88)
SO	0.5185(1.98)	-	0.4060(1.95)
SeO	0.6016(1.94)	-	0.3813(1.95)
SeS	0.7040(1.93)	-	0.3926(1.95)
BC	0.4991(1.87)	0.1627(1.02)	0.2420(0.97)
BC ⁻	0.4723(1.96)	0.1531(1.66)	0.5349(1.86)
PN	0.4613(1.98)	-	0.5978(1.90)
AsN	0.6054(1.98)	-	0.5736(1.89)
BeF	0.1602(1.98)	0.1421(1.00)	0.0755(1.98)
BeCl	0.2024(1.95)	0.1429(1.00)	0.0809(1.97)
BF	0.2169(1.98)	0.2818(1.88)	0.1372(1.97)
BCl	0.3280(1.95)	0.2496(1.88)	0.1670(1.97)

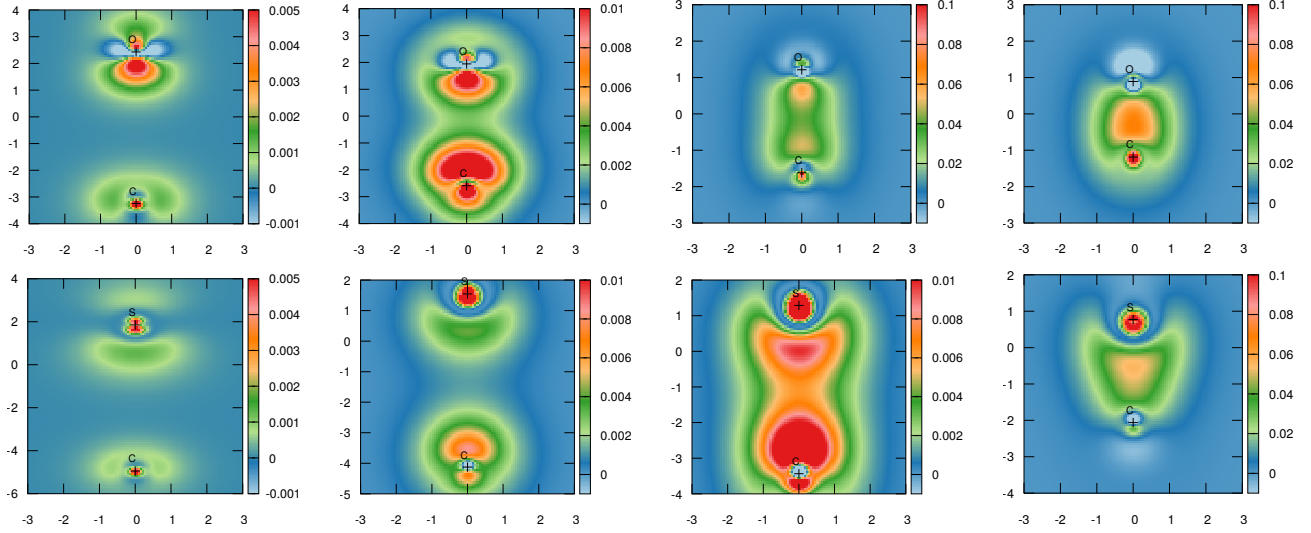


Figure 6: BOD maps of CO (top) and CS (bottom) molecules at decreasing internuclear distances. From left to right $R = 3.0, 2.4, 1.5, 1.10$ Å for CO and $R = 3.6, 3.0, 2.4, 1.5$ Å for CS. Notice that the color scales change with distance as the densities increase.

Table 8: Evolution of the dominant BODs of CO with the distance.

R (Å)	σ	exo- σ	$\pi_x = \pi_y$
1.1	0.3999(1.99)	0.2217(1.98)	0.4651(1.96)
1.5	0.5941(1.99)	0.0960(1.92)	0.4257(1.90)
2.4	0.2398(1.98)	0.0386(1.95)	0.1271(1.54)
3.0O	0.0366(1.98)	-	-0.0021(1.06)
3.0C	-	0.0169(1.97)	0.0010(0.94)

Table 9: Evolution of the dominant BODs of CS with the distance.

R (Å)	σ	exo- σ	$\pi_x = \pi_y$
1.5	0.6676(1.99)	0.0932(1.94)	0.6094(1.93)
2.4	0.4413(1.98)	0.0725(1.94)	0.2677(1.75)
3.0	0.1582(1.97)	0.0452(1.58)	0.0835(1.47)
3.6S	0.0463(1.95)	-	0.0016(1.05)
3.6C	-	0.0145(1.94)	0.0068(0.95)

Table 10: Evolution of the delocalization index δ^{AB} , covalent (E_{Cov}) and classical (E_{Cl}) interaction energy components, and net charges (Q_C, Q_O) of the CO molecule along the dissociation path.

Distance	δ^{AB}	E_{Cov}	E_{Cl}	Q_C	Q_O
0.9	1.5338	-0.5392	-1.7612	1.4251	-1.4244
1.0	1.4761	-0.4844	-1.6374	1.3484	-1.3485
1.1	1.4423	-0.4446	-1.4360	1.2600	-1.2594
1.2	1.3682	-0.3994	-1.1682	1.1540	-1.1540
1.3	1.3724	-0.3804	-0.8454	1.0056	-1.0054
1.4	1.3888	-0.3676	-0.4423	0.7809	-0.7802
1.5	1.3549	-0.3416	-0.2033	0.5950	-0.5949
1.6	1.2421	-0.3003	-0.1245	0.5034	-0.5029
1.7	1.1270	-0.2594	-0.0837	0.4388	-0.4381
1.8	1.0325	-0.2253	-0.0596	0.3879	-0.3880
1.9	0.9424	-0.1950	-0.0433	0.3437	-0.3436
2.0	0.8549	-0.1681	-0.0310	0.3007	-0.3008
2.1	0.7654	-0.1435	-0.0212	0.2562	-0.2562
2.2	0.6706	-0.1204	-0.0136	0.2103	-0.2100
2.3	0.5720	-0.0988	-0.0080	0.1650	-0.1650
2.4	0.4744	-0.0794	-0.0045	0.1250	-0.1252
2.5	0.3836	-0.0624	-0.0024	0.0922	-0.0920
2.6	0.3048	-0.0485	-0.0013	0.0657	-0.0657
2.7	0.2383	-0.0373	-0.0008	0.0453	-0.0454
2.8	0.1778	-0.0274	-0.0007	0.0260	-0.0259
2.9	0.1014	-0.0154	-0.0014	0.0011	-0.0010
3.0	0.0750	-0.0111	-0.0013	-0.0016	0.0015
3.1	0.0595	-0.0086	-0.0011	-0.0019	0.0019
3.2	0.0479	-0.0067	-0.0010	-0.0017	0.0018
3.4	0.0319	-0.0043	-0.0007	-0.0013	0.0013
3.6	0.0216	-0.0027	-0.0005	-0.0009	0.0009
3.8	0.0146	-0.0018	-0.0004	-0.0006	0.0005
4.0	0.0099	-0.0011	-0.0003	-0.0003	0.0003
4.2	0.0067	-0.0007	-0.0002	-0.0001	0.0001
4.4	0.0046	-0.0005	-0.0002	-0.0000	0.0000

Evolution of bonding densities

Bond order densities are very useful to follow different chemical processes. We compare here the results for CO and CS molecules along their respective dissociation curves, and analyze the isomerization of HCN into CNH.

CO versus CS

BODs here defined can be obtained equally well at the equilibrium or far from the equilibrium geometry, thus being well suited to study bond formation or bond breaking processes. To show their ability to uncover chemical rearrangements, we comment on the formation of the CO and CS molecules. Data are reported in Tables 8, 9, 10, and 11, and in Fig. 6.

As we approach the C and O atoms together, up to about $R = 2.9 \text{ \AA}$, there is a main bonding σ channel that can be assigned to a polarized $2p_z$ oxygen lone pair. The oxygen is still a local triplet, that is borne by π symmetry contributions. The carbon atom is also a local triplet, with a rather localized, unhybridized $2s$ function. In this regime, bonding is dative-like, and the carbon atom is (very slightly) negatively charged. The π channels do not contribute much to the overall bond order, although it is clear that the C atom small contribution is π -like.

A considerable electron reorganization occurs if R is reduced below $R = 2.8 - 3.0 \text{ \AA}$. The σ contribution now includes the heavy involvement of a C hybrid. This is possibly related to an avoided crossing on the energy surface. As the C atom becomes involved in electron-pair sharing, its $2s$ NAdO is polarized (or hybridized) and starts engaging in the exo-bond that survives to equilibrium. Simultaneously, π sharing starts. After this change, the O atom becomes negatively charged. At distances close to equilibrium the π eigenvalues are dominant, and the exo-link is transformed into a very important bonding actor. An oxygen lone-pair is also formed that is highly localized on the O atom.

In the CS molecule it is also a $3p_z$ S channel that starts a dative-like interaction at large distances. As R decreases the C atom becomes more negatively charged. This happens until at about

Table 11: Evolution of the delocalization index δ^{AB} , covalent (E_{Cov}) and classical (E_{Cl}) interaction energy components, and net charges (Q_C, Q_S) of the CS molecule along the dissociation path.

Distance	δ^{AB}	E_{Cov}	E_{Cl}	Q_C	Q_S
1.2	2.1299	-0.6484	-2.1188	-1.7887	1.7885
1.3	2.0607	-0.6032	-1.6464	-1.5241	1.5231
1.4	1.9828	-0.5604	-1.1879	-1.2492	1.2483
1.5	1.8936	-0.5178	-0.7568	-0.9598	0.9593
1.6	1.7878	-0.4726	-0.3409	-0.6272	0.6263
1.7	1.6255	-0.4104	0.0418	-0.1037	0.1041
1.8	1.5114	-0.3618	0.0352	-0.0242	0.0235
1.9	1.4031	-0.3184	0.0247	0.0161	-0.0162
2.0	1.2993	-0.2800	0.0164	0.0394	-0.0392
2.1	1.1988	-0.2458	0.0103	0.0533	-0.0536
2.2	1.0996	-0.2150	0.0062	0.0609	-0.0612
2.3	1.0011	-0.1870	0.0036	0.0638	-0.0636
2.4	0.9047	-0.1618	0.0019	0.0625	-0.0625
2.5	0.8089	-0.1389	0.0009	0.0579	-0.0577
2.6	0.7139	-0.1181	0.0004	0.0505	-0.0507
2.8	0.5260	-0.0818	0.0001	0.0317	-0.0314
3.0	0.3631	-0.0539	0.0000	0.0141	-0.0141
3.2	0.1855	-0.0262	-0.0012	-0.0211	0.0212
3.4	0.1137	-0.0154	-0.0012	-0.0162	0.0163
3.6	0.0766	-0.0099	-0.0010	-0.0110	0.0110
3.8	0.0529	-0.0066	-0.0008	-0.0074	0.0074
4.0	0.0369	-0.0044	-0.0006	-0.0049	0.0049

$R \approx 3.1 \text{ \AA}$ where the full σ is formed and the S atom becomes negatively charged. At smaller distances the system evolves much like in CO but a rehybridization occurs quite suddenly at about $R = 1.7 \text{ \AA}$, which changes polarity again, depleting the S valence. At equilibrium, a very localized $2s$ -like NAdO has appeared on C, and a more delocalized contribution lies on S. Overall, the carbon atom bears a considerable negative charge.

Isomerization of HCN

The isomerization of HCN into CNH is a thoroughly studied process that was used years ago to show that the exchange-correlation energies in the IQA approach were actually determining the formation of bond critical points in the topology of the electron density.¹⁶ We have now determined the H–C and H–N BODs that overall offer the same picture. HCN is in our calculation 17.5 kcal/mol more stable than CNH, and the transition state occurs at $\angle HCN \approx 79^\circ$. There is only one dominant σ -like channel for both the H–C and H–N BODs at any point along the transition. Table 12 shows their evolution. A sharp transition between a H–C dominant and a H–N dominant channel is clearly appreciated close to the transition state. Notice also that the endpoints are not symmetric: the H–C link in HCN is considerably more covalent than the H–N bond in CNH, see the SI.

Table 12: Main bond channel contribution of the H–C and H–N links during the isomerization process of HCN to CNH, as sensed by the H-C-N angle

$\angle HCN(^{\circ})$	H–C	H–N
180.0	0.395	0.054
133.0	0.376	0.065
87.2	0.284	0.140
70.3	0.133	0.257
49.3	0.069	0.291
0.0	0.025	0.300

Polyatomics

C_2H_2 versus Si_2H_2

The marked structural and chemical differences between alkynes and silynes have been thoroughly studied in recent years.^{44,45} Here we simply show the power of our approach to distinguish between these two bonding situations. The minimum energy isomer of Si_2H_2 has a well-known C_{2v} dibridged geometrical arrangement. No $D_{\infty h}$ isomer is stable, but a C_{2h} trans isomer is closest to the acetylene geometry. To compare these two molecules, we consider the links between two equivalent CH or SiH (AH) neutral groups. In this way we smooth out electronegativity differences, since the charges of C and Si are -0.134 and $+0.691 e$, respectively. The internuclear MP is in both cases a maximum of the BOD, with values equal to 0.086 and 0.017 au, respectively. Ignoring minor channels and negative correlating contributions, both systems display three independent AH–AH bonding channels. In acetylene these are the standard $\sigma + 2\pi$ canonical bonds, with $2n^{ab} = 0.798, 0.622, 0.622$, respectively. Notice that, as already shown in Table 5, both the σ and π channels in C_2H_2 are among the strongest found in our survey. If we now change to C_{2h} silyne, the σ channel is about 15% bit weaker, similar to that in diboron, with an eigenvalue 0.631 . A clear π channel, orthogonal to the molecular plane, is also present, with $2n^{ab} = 0.516$ (20% weaker). In some approaches, like that provided by the ELF function,⁴⁶ two quasi lone pairs appear in the molecular plane centered on each Si atom, and a double-bonded system is inferred. However, we actually find a third weaker π -like bond channel in the molecular plane (see Fig. 7) with occupation 0.302 . This is formed through the delocalization of the Si lone pairs into the H regions. Notice that this is in agreement with the tendency of H atoms to form bridged structures in this system. We think that this kind of insight is difficult to obtain by other methodologies. An analysis of the minimum energy isomer (C_{2v}) leads to only one σ channel between the two Si atoms, with an eigenvalue equal to 0.537 (0.583 in the trans case). The H atoms are slightly more negatively charged (-0.729 au), and clearly engaged in standard $3c,2e$ bonds. Two clear Si $2s$ -like lone pairs appear.

$\text{NH}_3 \rightarrow \text{BH}_3$

The adduct between BH_3 and NH_3 is taken as the paradigm of a dative bond. At the equilibrium geometry, the acceptor BH_3 molecule is negatively charged, $Q = -0.073$ au, and our analysis shows a dominant σ channel that contributes 0.374 to the total inter-fragment DI. However, since the hydridic H atoms of the borane moiety bear a rather negative charge (-0.694 au each), their overlap and thus total delocalization over the ammonia fragment is not negligible, contributing overall with 0.324 to the DI. Smaller ammonia contribution add to about 0.1. Indirect delocalizations may play a role that may have not been adequately considered in the literature.

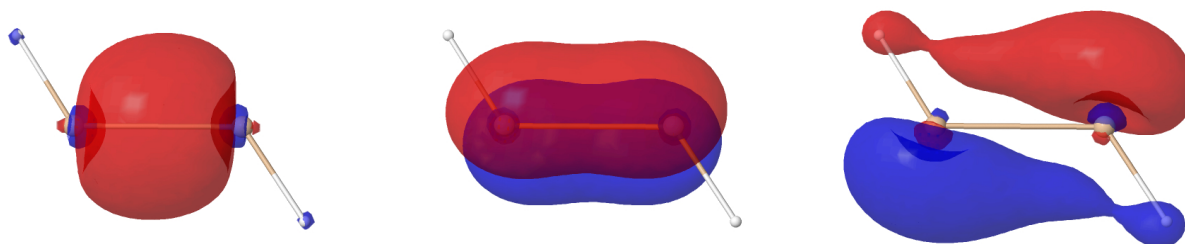


Figure 7: The three main bonding NAdOs of $\text{trans-Si}_2\text{H}_2$. The isosurface 0.064 au is plotted.

CH_2N_2

We can also understand how the N–N bond weakens after forming CH_2N_2 . Considering the link between the two N atoms, we first observe that the total N–N DI decreases to 1.724. A NAdOs/BOD analysis shows that all the dominant channels have weakened: the σ eigenvalue is now 0.737. Amongst the π contributions, it is the one orthogonal to the molecular plane that suffers the largest weakening, falling to 0.499, while the perpendicular one stays at 0.576.

Bond order densities in excited states

BODs can equally be obtained in excited states, where they can offer unique bonding insights given that many of the rules governing the chemistry of ground states cannot be easily generalized to excited states (ESs). We have shown in the last years that although the presence of non-nuclear maxima, for instance, was thought to preclude the application of the QTAIM to ESs, in many situations this is not true, and that most non-Rydberg states possess standard atomic basins.^{22,47} Recently, it has been shown that the full DI landscape is more complex than initially thought, with DIs that may be negative or greater than one for 2c,2e cases if ESs are included.²²

We have first selected the $B^1\Sigma_u^+$ (S1) and the double minimum $E,F^1\Sigma_g^+$ (S2) states of dihydrogen at the MRCI-SD level of theory with a two-orbital 10-electron reference obtained from a state averaged wavefunction (SA-CASSCF) with the d-aug-cc-pVDZ³³ basis set. The S1 state has a minimum at 1.27 Å with $DI \approx 1.304$. This larger than one value points to a zwitterionic character of the state, as we have already noticed.²² We have found two degenerate channels, each contributing 0.645 to the DI. They have σ_g and σ_u symmetries and can be obviously localized to form 1s-atomic like NAdOs. The S2 state has two minima (E,F). The E minimum is located at $R = 1.02$ Å, with $DI \approx 0.921$. There are again two channels, this time asymmetric with $2n^{ab}$ equal to 0.533 and 0.384, respectively. The first NAdO is a $\sigma_g(1s)$ function, while the second, clearly more diffuse, is a $\sigma_g(2s)$ function. This is appealing, since the E state correlates with the $\sigma_g(1s)^1\sigma_g(2s)^1$ configuration and its dissociation products are a 1s H atom and a 2s H atom.⁴⁷ The F state is again zwitterionic (correlating with the ionic resonance at dissociation) with $DI = 1.496$. The minimum is located at $R = 2.14$ Å, and the two main channels are asymmetric. The σ_g one contribution is 0.616 while the σ_u one is larger, 0.780.

A final introductory example we have investigated is the first excited state of H_4 in the D_{4h} geometry. We have convincingly shown²² after a full configuration interaction calculation that the DIs between diagonally opposed H atoms become clearly negative over a wide range of H–H distances in the first excited $^1A_{1g}$ state. At $R_{H-H} = 1.2$ Å, the DI between adjacent H atoms is 0.512, with one main σ channel contributing 0.378 and two opposing correlating ones that involve the

other two atoms. Contrarily, the DI between the diagonally opposed H atoms is -0.049 , consisting of two positive ($0.049, 0.039$) and one zwitterionic negative (-0.137) contributions. The overall BOD for the adjacent and diagonal contributions are found on Fig. 8

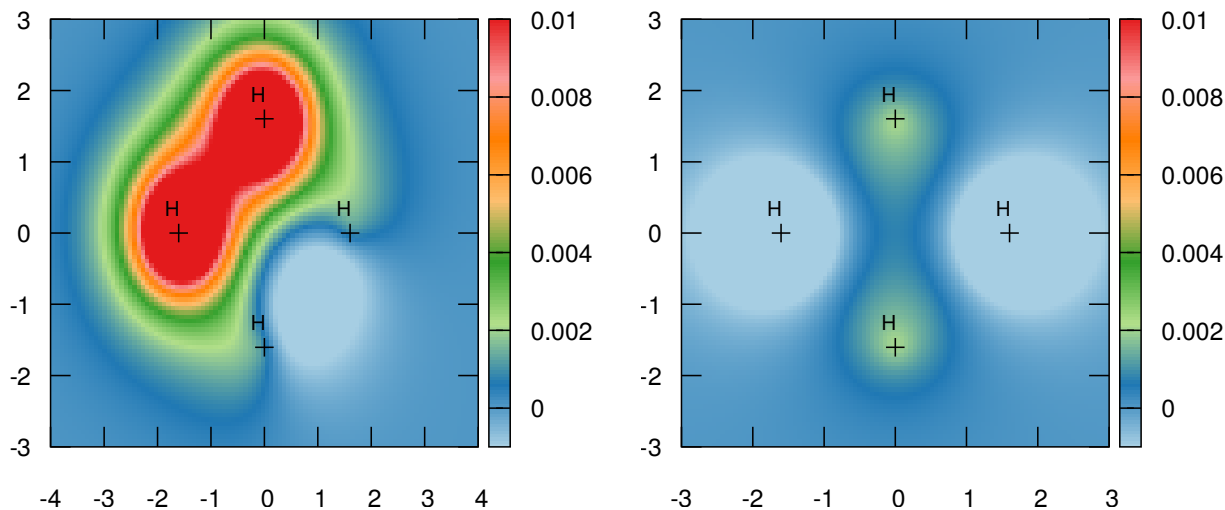


Figure 8: BODs of the adjacent (left) and diagonal (right) H–H links in the ${}^1A_{1g}$ excited state of H_4 at $R_{H-H} = 1.2 \text{ \AA}$.

Summary and conclusions

In this article, a new scalar field named bond order density (BOD) has been defined, which has proven to be a powerful tool to analyze the chemical bond from a real space perspective. BOD can be computed at any level of theory from the natural adaptive orbitals (NAdOs) of the system, introduced some years ago.^{6,14} Although obtaining the BODs from explicitly correlated wavefunctions is not trivial due to their dependence on the third order cumulant density (3CD), their computation in the mean field case is particularly simple. NAdOs in this case can be easily obtained from the atomic overlap matrices (AOM) between all the molecular orbitals of the system. From a formal point of view, this is also true in a Density Functional Theory (DFT) formalism, where Kohn-Sham orbitals can be used as well to obtain (in this order) the AOM, the NAdOs, and the BOD. Moreover, there is no limitation as to whether BODs are computed in ground or excited states, provided that the 3D space can be divided into different atomic domains.

The bond order density associated to a pair of atoms or functional groups can be diagonalized and, therefore, decomposed into as many contributions as the number of molecular orbitals of the system. Positive and negative eigenvalues signal bonding and *antibonding-like* channels respectively. Both the full BOD as well as any of its eigenvectors can be visualized, offering vivid images of the real space regions that contribute the most to the bond order between any two atoms of the molecule. Computing the BOD along an arbitrary reaction coordinate (for instance, the dissociation of a molecule into two fragments or an isomerization process) may offer very valuable information about how some chemical bonds are broken and others are formed or modified.

In this first exploratory work, we have focused in the analysis of the BOD scalar field and of its different channels for a number of homodiatomic and heterodiatomic molecules, and for C_2H_2 and Si_2H_2 , at their respective equilibrium geometries. The aim has been to gain insight on the distribution, character, and intensity of their chemical bonding. The BODs of the CO and CS molecules along their dissociation curves have also been computed and compared to each other. We have also studied the evolution of the BOD along the isomerization process of HCN into CNH. Finally, bond order densities have been computed and analyzed for a couple of excited electronic states of H_2 and the first excited state ($^1A_{1g}$) of H_4 in the D_{4h} geometry.

A number of lessons can be learnt from analyzing BODs. In textbook examples, like the second period homodiatomics, the mean-field image provides a picture close to the molecular orbital paradigm with, for instance, three bonds (channels) in dinitrogen. Even in these archetypal systems some interesting facts arise: the $2\sigma_g$ and $2\sigma_u$ orbitals do not cancel out completely, and extra- σ channels survive, as in the NBO approach. These exo-bonds are clearly, but not only, found in di-carbon. Electron correlation usually introduces small changes, although not always. The weakening effect of lone pairs, for instance, is clearly visible as we move through the period, being maximum in F_2 , where regions with negative BODs cannot be overlooked. Since the BOD machinery can be used at any level of theory, BODs are particularly relevant to ascertain and understand the role of correlation on particular chemical bonds. Moreover, sometimes non-traditional channels contributing non-negligibly to electron delocalization among atoms or fragments appear. This is

the case in the ammonia borane complex, where the borane hydridic moieties play a clear role in bonding. The BOD analysis clearly shows that the total bond order is not necessarily correlated to the number of independent contributions to it. A total DI of 1, for instance, may be the result of a larger number of weaker components, thus involving a non-negligible multiple bond character to the link.

The BOD here introduced thus provides unique insights into the different bonding contributions that add to the real space bond order. It is particularly useful to analyze correlated wavefunctions, where traditional molecular orbital techniques quickly lose their meaning. This is so because the number of bonding channels participating in a chemical link is usually low and reminiscent of that found in the mean field case, so that the BOD technique easily maps the independent particle picture to the fully correlated one.

Conflicts of interest

There are no conflicts to declare.

Supporting information

Cartesian coordinates of HCN and CH₂N₂, BOD maps for all bonding channels of heterodiatomics and homodiatomics in alphabetical order. This material is available free of charge via the internet at <http://pubs.acs.org>

Acknowledgements

We thank the Spanish MICINN, grant PGC2018-095953-B-I00, the FICYT, grant IDI/2018/000177, and the European Union FEDER funds for financial support.

References

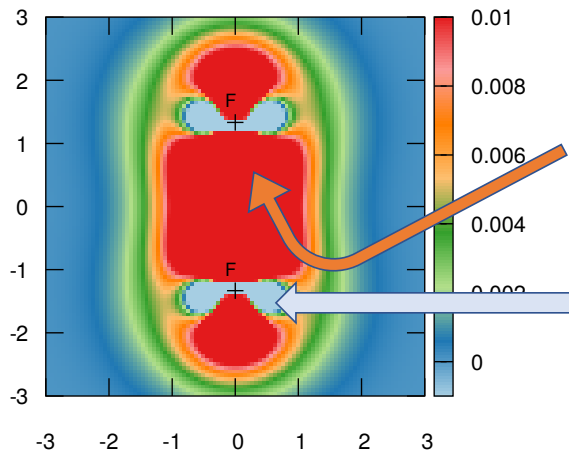
- (1) Popelier, P. L. A.; Brèmond, E. A. Geometrically Faithful Homeomorphisms between the Electron Density and the Bare Nuclear Potential. *Int. J. Quant. Chem.* **2009**, *109*, 2542–2553.
- (2) Gimarc, B. M. *Molecular structure and bonding. The qualitative molecular orbital approach*; Academic Press: New York, 1979.
- (3) Shaik, S.; Maitre, P.; Sini, G.; Hiberty, P. C. The charge-shift bonding concept. Electron-pair bonds with very large ionic-covalent resonance energies. *Journal of the American Chemical Society* **1992**, *114*, 7861–7866.
- (4) Martín Pendás, A.; Francisco, E. Real space bond orders are energetic descriptors. *Phys. Chem. Chem. Phys.* **2018**, *20*, 16231–16237.
- (5) Roos, B. O.; Lindh, R.; Malmqvist, P.-A.; Veryazov, V.; Widmark, P.-O. Main Group Atoms and Dimers Studied with a New Relativistic ANO Basis Set. *J. Phys. Chem. A* **2004**, *108*, 2851–2858.
- (6) Menéndez, M.; Álvarez Boto, R.; Francisco, E.; Martín Pendás, Á. One-electron images in real space: Natural adaptive orbitals. *J. Comput. Chem.* **2015**, *36*, 833–843.
- (7) Francisco, E.; Martín Pendás, A.; García-Revilla, M.; Álvarez Boto, R. A Hierarchy of Chemical Bonding Indices in Real Space from Reduced Density Matrices and Cumulants. *Comput. Theor. Chem.* **2013**, *1003*, 71–78.
- (8) Zubarev, D. Y.; Boldyrev, A. I. Developing Paradigms of Chemical Bonding: Adaptive Natural Density Partitioning. *Phys. Chem. Chem. Phys.* **2008**, *10*, 5207–5217.
- (9) Martín Pendás, A.; Francisco, E. From quantum fragments to Lewis structures: electron counting in position space. *Phys. Chem. Chem. Phys.* **2018**, *20*, 21368–21380.
- (10) Francisco, E.; Martín Pendás, A.; Blanco, M. A. Electron Number Probability Distributions for Correlated Wave Functions. *J. Chem. Phys.* **2007**, *126*, 094102–1–094102–13.

- (11) Blanco, M. A.; Martín Pendás, A.; Francisco, E. Interacting Quantum Atoms: A Correlated Energy Decomposition Scheme Based on the Quantum Theory of Atoms in Molecules. *J. Chem. Theory Comput.* **2005**, *1*, 1096–1109.
- (12) Francisco, E.; Martín Pendás, A.; Blanco, M. A. A Molecular Energy Decomposition Scheme for Atoms in Molecules. *J. Chem. Theory Comput.* **2006**, *2*, 90–102.
- (13) Martín Pendás, A.; Francisco, E. Chemical Bonding from the Statistics of the Electron Distribution. *ChemPhysChem* **2019**, *20*, 1–21.
- (14) Francisco, E.; Martín Pendás, A.; García-Revilla, M.; Álvarez Boto, R. A Hierarchy of Chemical Bonding Indices in Real Space from Reduced Density Matrices and Cumulants. *Comput. Theor. Chem.* **2013**, *1003*, 71–78.
- (15) Bader, R. F. W. *Atoms in molecules: A Quantum Theory*; Oxford University Press, 1990.
- (16) Martín Pendás, A.; Francisco, E.; Blanco, M. A.; Gatti, C. Bond paths as privileged exchange channels. *Chem. Eur. J.* **2007**, *13*, 9362–9372.
- (17) Outeiral, C.; Vincent, M. A.; Martín Pendás, A.; Popelier, P. L. A. Revitalizing the concept of bond order through delocalization measures in real space. *Chem. Sci.* **2018**, *9*, 5517–5529.
- (18) Bader, R. F. W.; Stephens, M. E. Fluctuation and Correlation of Electrons in Molecular Systems. *Chem. Phys. Lett.* **1974**, *26*, 445–449.
- (19) Giambiagi, M.; de Giambiagi, M. S.; Mundim, K. C. Definition of a multicenter bond index. *Struct. Chem.* **1990**, *1*, 423–427.
- (20) Mundim, K. C.; Giambiagi, M.; de Giambiagi, M. S. Multicenter Bond Index: Grassmann Algebra and N-Order Density Functional. *J. Phys. Chem.* **1994**, *98*, 6118–6119.
- (21) Andrada, D. M.; Casals-Sainz, J. L.; Martín Pendás, Á.; Frenking, G. Dative and Electron-Sharing Bonding in C₂F₄. *Chem. Eur. J.* **2018**, *24*, 9083–9089.

- (22) Casals-Sainz, J. L.; Jara-Cortés, J.; Hernández-Trujillo, J.; Guevara-Vela, J. M.; Francisco, E.; Martín Pendás, A. Exotic Bonding Regimes Uncovered in Excited States. *Chem. Eur. J.* **2019**, *25*, 12169–12179.
- (23) Francisco, E. Denmat. A cumulant analysis code (Available from the authors upon request).
- (24) Martín Pendás, A.; Francisco, E. Promolden. A QTAIM/IQA code (Available from the authors upon request.).
- (25) Linstrom, P. J., Mallard, W. G., Eds. *NIST Chemistry WebBook, NIST Standard Reference Database Number 69*; National Institute of Standards and Technology: Gaithersburg MD, 20899, 2017.
- (26) Magoulas, I.; Kalemou, A.; Mavridis, A. An ab initio study of the electronic structure of BF and BF+. *J. Chem. Phys.* **2013**, *138*, 104312.
- (27) Magoulas, I.; Kalemou, A. An ab initio study of the electronic structure of the boron oxide neutral (BO), cationic (BO+), and anionic (BO-) species. *J. Chem. Phys.* **2014**, *141*.
- (28) Polák, R.; Fišer, J. A comparative icMRCI study of some NO+, NO and NO-electronic ground state properties. *Chem. Phys.* **2004**, *303*, 73–83.
- (29) Ornellas, F.; Machado, F.; Roberto-Neto, O. A theoretical study of the molecules bef and bef+ in their lowest-lying electronic states. *Mol. Phys.* **1992**, *77*, 1169–1185.
- (30) Sayfutyarova, E. R.; Sun, Q.; Chan, G. K.-L.; Knizia, G. Automated construction of molecular active spaces from atomic valence orbitals. *J. Chem. Theory Comput.* **2017**, *13*, 463–478.
- (31) Noro, T.; Sekiya, M.; Koga, T. Segmented contracted basis sets for atoms H through Xe: Sapporo-(DK)-nZP sets (n = D, T, Q). *Theor. Chem. Acc.* **2012**, *131*, 1–8.
- (32) Sun, Q.; Berkelbach, T. C.; Blunt, N. S.; Booth, G. H.; Guo, S.; Li, Z.; Liu, J.; McClain, J. D.; Sayfutyarova, E. R.; Sharma, S. et al. PySCF: the Python-based simulations of chemistry framework. *WIREs Comput. Mol. Sci.* **2018**, *8*, e1340.

- (33) Dunning, T. H. Gaussian basis sets for use in correlated molecular calculations. I. The atoms boron through neon and hydrogen. *J. Chem. Phys.* **1989**, *90*, 1007–1023.
- (34) Schmidt, M. W.; Baldridge, K. K.; Boatz, J. A.; Elbert, S. T.; Gordon, M. S.; Jensen, J. H.; Koseki, S.; Matsunaga, N.; Nguyen, K. A.; Su, S. et al. General atomic and molecular electronic structure system. *J. Comput. Chem.* **1993**, *14*, 1347–1363.
- (35) Werner, H.-J.; Knowles, P. J.; Knizia, G.; Manby, F. R.; Schütz, M. Molpro: a general purpose quantum chemistry program package. *WIREs Comput. Mol. Sci.* **2012**, *2*, 242–253.
- (36) Francisco, E.; Martín Pendás, A.; Blanco, M. EDF: Computing electron number probability distribution functions in real space from molecular wave functions. *Comput. Phys. Commun.* **2008**, *178*, 621 – 634.
- (37) Reed, A. E.; Curtiss, L. A.; Weinhold, F. Intermolecular Interactions from a Natural Bond Orbital, Donor–Acceptor Viewpoint. *Chem. Rev.* **1988**, *88*, 899–926.
- (38) Reed, A. R.; Weinhold, F. Natural Bond Orbital Analysis of Near-Hartree-Fock Water Dimer. *J. Chem. Phys.* **1983**, *78*, 4066–4073.
- (39) Reed, A. R.; Weinhold, F.; Curtiss, L. A.; Pochatko, D. J. Natural Bond Orbital Analysis of Molecular Interactions: Theoretical Studies of Binary Complexes of HF, H₂O, NH₃, N₂, O₂, F₂, CO, and CO₂ with HF, H₂O, and NH₃. *J. Chem. Phys.* **1986**, *84*, 5687–5705.
- (40) Weinhold, F.; Landis, C. *Valency and Bonding. A Natural Bond Orbital Donor-Acceptor Perspective*; Cambridge Univ. Press, 2005.
- (41) Shaik, S.; Danovich, D.; Braida, B.; Hiberty, P. C. The Quadruple Bonding in C₂ Reproduces the Properties of the Molecule. *Chem. Eur. J.* **2016**, *22*, 4116–4128.
- (42) Sanderson, R. T. *Polar Covalence*; Academic Press: New York, 1983.
- (43) Silvi, B.; Savin, A. Classification of chemical bonds based on topological analysis of electron localization functions. *Nature* **1994**, *371*, 683–686.

- (44) Malcolm, N. O. J.; Gillespie, R. J.; Popelier, P. L. A. A topological study of homonuclear multiple bonds between the elements of group 14. *J. Chem. Soc., Dalton Trans.* **2002**, 3333–3341.
- (45) Power, P. P. Bonding and Reactivity of Heavier Group 14 Element Alkyne Analogues. *Organometallics* **2007**, *26*, 4362–4372.
- (46) Becke, A. D.; Edgecombe, K. E. A simple measure of electron localization in atomic and molecular systems. *J. Chem. Phys.* **1990**, *92*, 5397–5403.
- (47) Jara-Cortés, J.; Guevara-Vela, J. M.; Martín Pendás, Á.; Hernández-Trujillo, J. Chemical bonding in excited states: Energy transfer and charge redistribution from a real space perspective. *J. Comput. Chem.* **2017**, *38*, 957–970.



Bond order density in F_2

Positive contribution to the DI
Fermi correlation dominates

Negative contribution to the DI
Coulomb correlation dominates